Int J Adv Manuf Technol (2017) 92:2401–2410
DOI 10.1007/s00170-017-0295-0

ORIGINAL ARTICLE

Effect of rotation speed on nugget structure and property of high rotation speed friction stir welded Al-Mn aluminum alloy

H. J. Zhang[1] · M. Wang[1] · R. L. Qi[1] · Z. Zhu[1] · X. Zhang[1] · T. Yu[1] · Z. Q. Wu[1]

Received: 6 October 2016 / Accepted: 13 March 2017 / Published online: 1 April 2017

Abstract High rotation speed friction stir welding is a promising low-force welding technique that enables the application of friction stir welding on in situ fabrication and repair. High rotation speed friction stir welding experiments (above 3000 rpm) were conducted on an Al-Mn aluminum alloy. The effect of rotation speed on nugget structure and property was investigated in order to illuminate the process features. The results indicate that a notable increase of nugget size occurs at high rotation speeds of 5000–8000 rpm. With increasing rotation speed, the thermal effect is firstly strengthened and then achieves a steady state. The microstructure evolution is more sensitive to welding temperature as rotation speed varies, and thus, the evolution trends of nugget structure morphology (grain size and substructure distribution density) with rotation speed resemble that of welding temperature. Increasing rotation speed above 4000 rpm effectively improves the nugget hardness due to the enhancement of strain hardening.

Keywords High rotation speed friction stir welding · Rotation speed · Weld nugget · Structure · Property

1 Introduction

Friction stir welding (FSW) is a solid-state joining process, during which the weld is formed under the thermal and mechanical effects exerted by a rotating tool [1]. The rotation speed of the welding tool is an important control variable of heat generation during FSW [2]. Traditionally, the rotation speeds less than 3000 rpm were applied to welding tool during FSW [3]. In recent years, FSW conducted at much higher rotation speeds (above 3000 rpm) has attracted more and more attention. The primary advantage of high rotation speed FSW (HRS-FSW) is the ability to reduce the welding forces during FSW [4]. Compared with the heavy-duty welding machines used in conventional FSW (C-FSW), HRS-FSW makes it possible to implement FSW with light-weight and small-scale welding machines and thus promotes the application of the advanced welding technique on in situ fabrication and repair [5]. Owing to this, the HRS-FSW process was even considered as a potential basis for handheld manual welding technique in space by the NASA Marshall Space Flight Center [6].

The requirement of low-force FSW technique allows the development of HRS-FSW. In contrast to C-FSW, the reduced forging loads during HRS-FSW tend to create more opportunities for the occurrence of defects in the welds. For example, Banwasi et al. [7] performed HRS-FSW on a 1.5-mm-thick 2024-T3 aluminum alloy in a high rotation speed range of 6000–24,000 rpm. It was found that a number of weld defects including voids, wormholes, and porosity were commonly observed in the joints. Owing to this, the earlier research related to HRS-FSW was mainly focused on material flow control and weld quality improvement. Widener et al. [8] introduced a fixed shoulder surrounding the rotating pin to the welding tool when conducting the FSW experiments on a 3.2-mm-thick 6061-T4 aluminum alloy at the rotation speed of 15,000 rpm. A defect-free joint with the joint efficiency of 0.85 was obtained by using the fixed-shouldered tool. Nicholas et al. [9] also utilized the fixed-shouldered welding tool to conduct HRS-FSW on a 3.2-mm-thick 5456-H111

✉ R. L. Qi
qiruolong@sia.cn

[1] Shenyang Institute of Automation Chinese Academy of Sciences, State Key Laboratory of Robotics, Shenyang 110000, People's Republic of China

Table 1 Chemical compositions and mechanical properties of 3A21-O aluminum alloy

Chemical compositions (wt.%)								Mechanical properties		
Al	Mn	Si	Fe	Cu	Zn	Ti	Mg	Tensile strength	Elongation	Hardness
Bal.	1.0–1.6	0.6	0.7	0.2	0.1	0.15	0.05	115 MPa	20%	34–36 Hv

aluminum alloy at the rotation speed of 12,000 rpm, and defect-free joints with tensile strength equivalent to the base metal were successfully produced. In addition to these experimental studies, numerical analyses on HRS-FSW were also made by Crawford et al. [10]. The results revealed that the material would become more fluid like when the rotation speed was around 5000 rpm, which led to the decrease of welding loads dramatically.

Although there have been some investigations on HRS-FSW from the aspects of welding tool, weld formation, and joint properties over the past several years, the knowledge on HRS-FSW is still lacking. In particular, the effect of welding parameters on the HRS-FSW behavior is still largely uncharacterized. If the HRS-FSW process is to be optimized in the future, it is evidently important to understand the relationships between the process variables and the weld microstructures and mechanical properties in different zones.

For this reason, the HRS-FSW experiments were carried out on an Al-Mn aluminum alloy in this paper, and the influences of tool rotation speed on weld formation feature, welding thermal cycle, microstructure, and hardness distribution of the HRS-FSW joints were studied in detail. All of the zones of a friction stir weld, including the weld nugget zone, thermo-mechanically affected zone, and heat-affected zone, are clearly important in determining the overall properties of FSW joint; however, the main focus of the present investigation is placed on the nugget zone. This work is expected to help to illuminate the affecting features of tool rotation speed on the performances of HRS-FSW joints and thus to provide guidance for better understanding and application of the HRS-FSW process.

2 Experimental procedure

The base metal (BM) used for the experiment was a 5-mm-thick 3A21 aluminum alloy in annealed condition. It is a type of antirust aluminum alloy belonging to Al-Mn series and is widely used in aircraft industries. The chemical compositions and mechanical properties of the BM are listed in Table 1. The grains of the BM are characterized by coarse elongated morphologies (181 ± 41 μm in size) (see Fig. 1a), where the high-angle grain boundaries (HAGBs, the grain boundaries with the misorientation angle larger than 15°)

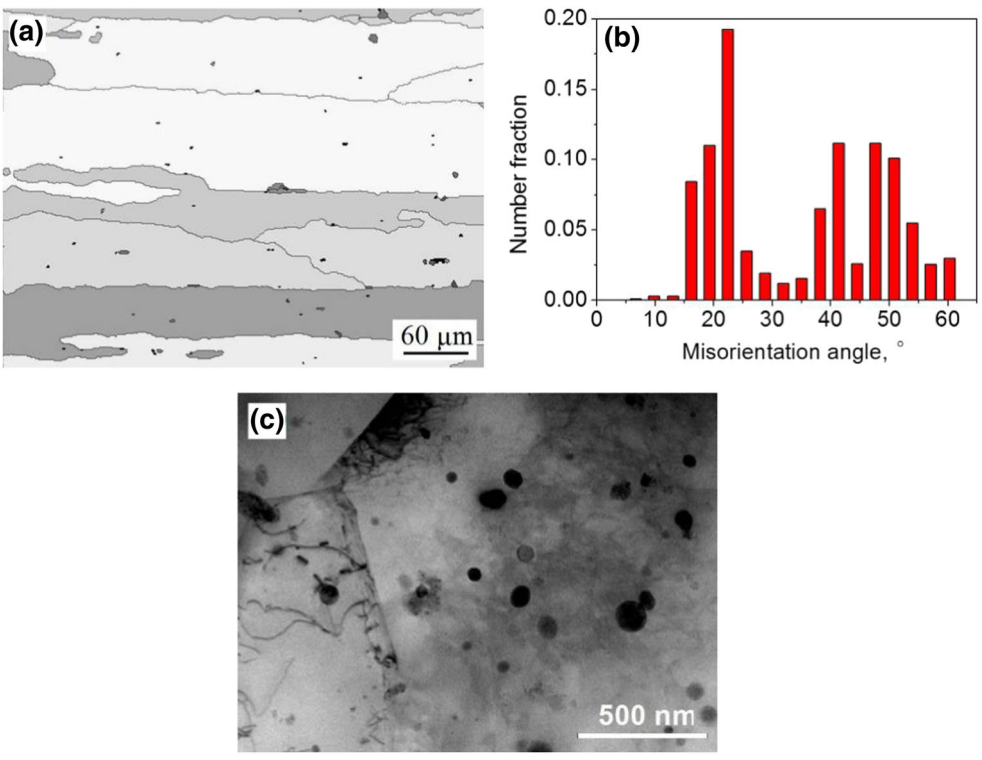

Fig. 1 Microstructures of the BM. **a** Grains. **b** Distribution of the misorientation angle. **c** Dislocations and second phase particles

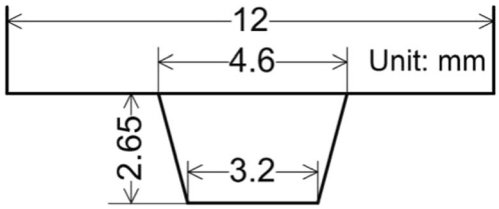

Fig. 2 Schematic diagram of the tool with dimensions

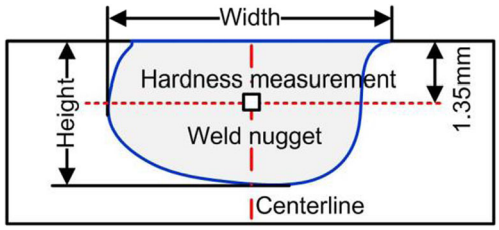

Fig. 3 Schematic view of the exact locations for structure-property analyses of HRS-FSW joints

account for a large number fraction of 91% (see Fig. 1b). The dislocation density of BM is rather low. Some Mn-rich second-phase particles are distributed in the matrix (see Fig. 1c). The dimension of welding samples was 150 mm long by 150 mm wide.

The welding tool used for HRS-FSW had a 12-mm-diameter shoulder with scrolls on the end surface. The scrolled shoulder with spiral channels cut from the shoulder edge toward the center had the ability to develop a strong inwardly directed traction force for the material flow and thus could help to prevent the slipping and expelling of plastic material from tool shoulder during HRS-FSW. The conical tool pin had right-hand threads for counterclockwise rotation. Our previous experimental trials found that the heights of weld nugget zones of HRS-FSW joints were significantly larger than the pin length. Therefore, a relatively short pin length of 2.65 mm was selected in the study in order to prevent the BM from sticking to the backing plate during the welding. The schematic diagram of the tool with dimensions is depicted in Fig. 2.

Bead-on-plate FSW experiments were carried out perpendicular to the rolling direction of the workpiece using a FSW machine. The tool rotation speed varied in the range of 1000–8000 rpm. The chosen rotation speeds included both the conventional rotation speed values (1000–2000 rpm) and the high rotation speed values (3000–8000 rpm). The welding speed was fixed at 25 mm/min. A 0.05-mm shoulder plunge depth and a zero tool tilt angle were applied to the welding tool. It is difficult to directly examine the welding temperature of the nugget zone using thermocouples due to the severe plastic deformation. Therefore, the welding thermal cycles at the workpiece bottom surface beneath the pin tip were measured during the welding to evaluate the thermal effect exerted by welding tool.

After welding, the joints were all cross-sectioned perpendicular to the welding direction for metallographic analyses and hardness tests. The cross sections of the metallographic specimens were polished using a diamond paste and etched with Keller's reagent to reveal the weld morphology. The microstructural analyses of weld nugget zone were made at the mid-thickness of tool penetration (1.35 mm from the workpiece top surface) along the weld centerline, as indicated by the small black square in Fig. 3. The Vickers hardness tests were performed at the mid-thickness of tool penetration on the weld cross sections by a microhardness tester, as shown by the short dotted line in Fig. 3. The spacing between the adjacent indentations was 1 mm, and the testing load was 1.96 N for 10 s. The block frame shown in Fig. 4 summarizes the experimental system with all input-output data. By conducting the analyses and tests on weld nuggets at different rotation speeds, the correlations between nugget performances and rotation speed are expected to be comprehensively clarified.

3 Results and discussion

3.1 Nugget morphologies

The weld cross sections observed by the optical microscopy (Olympus SZ61) are shown in Fig. 5. In the figure, the retreating side (RS) is on the left and the advancing side

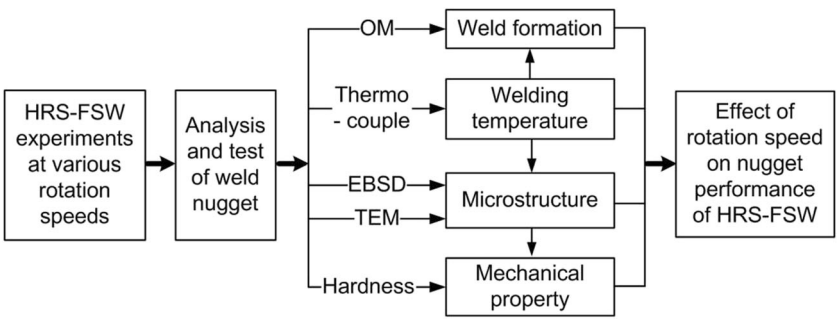

Fig. 4 Experimental system with all input-output data

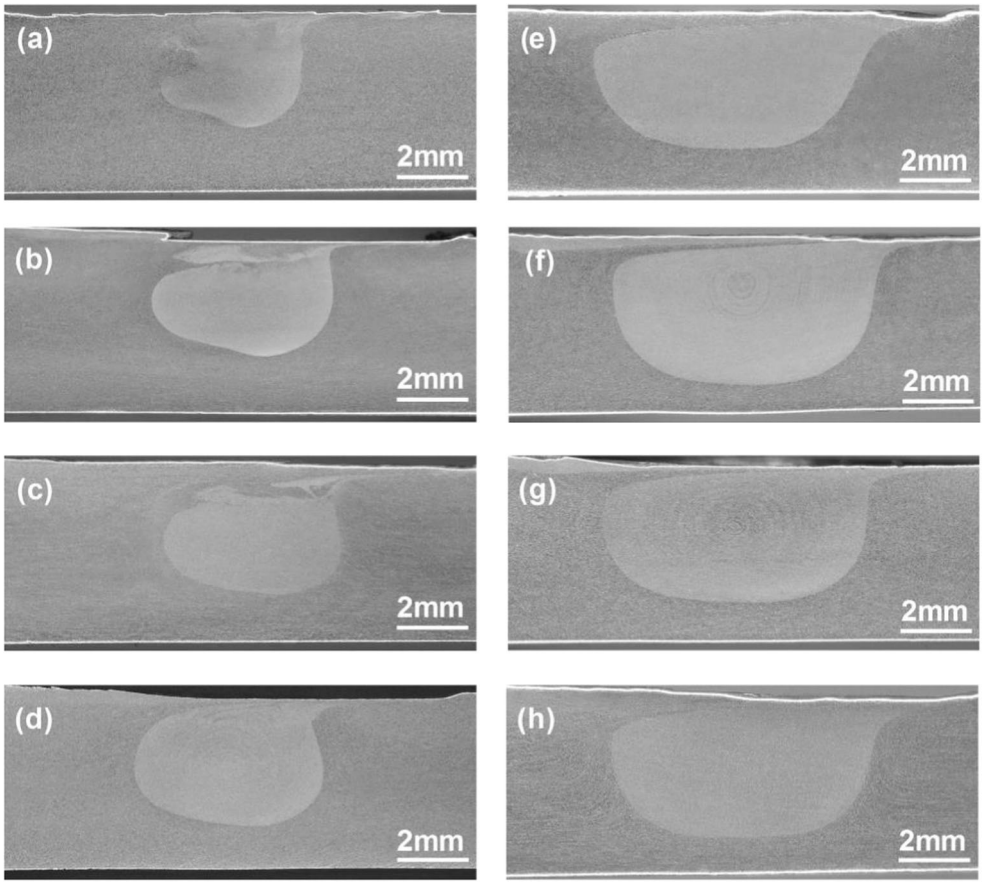

Fig. 5 Weld cross sections obtained at different rotation speeds. **a** 1000 rpm. **b** 2000 rpm. **c** 3000 rpm. **d** 4000 rpm. **e** 5000 rpm. **f** 6000 rpm. **g** 7000 rpm. **h** 8000 rpm

(AS) is on the right for each cross section. It can be seen that the defect-free joints are formed not only at the conventional rotation speeds (1000 and 2000 rpm) but also at the high rotation speeds (3000–8000 rpm), indicating that the tool used here is capable of effectively controlling the material flow during HRS-FSW. Obviously, the nugget size varies with rotation speed. According to the measurement method described in Fig. 3, the width and height of nugget zones are summarized in Fig. 6. Note that the pin diameter at tool shoulder and the pin length are also overlaid on the micrograph.

The nugget widths are in the range of 4.1–5.4 mm between 1000 and 4000 rpm, comparable with the pin diameter (4.6 mm), however, they are enlarged by about 4.5 mm at the rotation speeds ranging from 5000 to 8000 rpm. Large nugget width can also be formed in C-FSW of aluminum alloys. For instances, the nugget widths near to the shoulder diameter were separately attained by Doude et al. [11] in the 2219 aluminum alloy joint at 600 rpm and by Buchibabu et al. [12] in the RDE40 aluminum alloy joint at 450 rpm. However, it is difficult to observe such a large extent of nugget width increase when the rotation speed is improved at an interval of 1000 rpm in C-FSW. This implies that for HRS-FSW, a notable enhancement of material plastic flow can occur as the rotation speed reaches a certain high level due to the lowering of material flow stress.

The nugget height also roughly increases with increasing rotation speed. Between 5000 and 8000 rpm, the nuggets cover significantly larger depths than the pin length. The differences between the nugget heights and the pin length reach about 1.5 mm. Similar phenomenon also appeared in Widener et al.'s research on HRS-FSW [8]. They performed HRS-FSW on a 3.2-mm-thick 6061-T4 aluminum alloy at 15000 rpm using a tool with pin length of 1.4 mm. A clear secondary induced stir zone was formed below the pin,

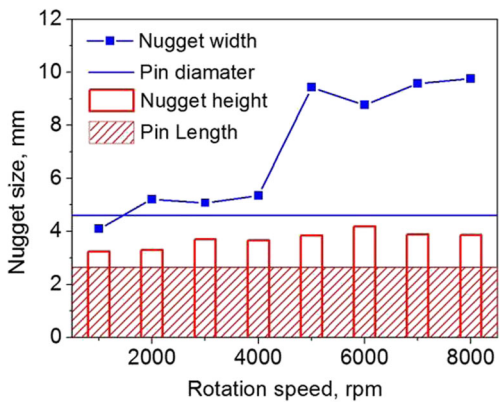

Fig. 6 Weld nugget size measured at different rotation speeds. Note that the pin diameter at tool shoulder and the pin length are overlaid on the micrograph

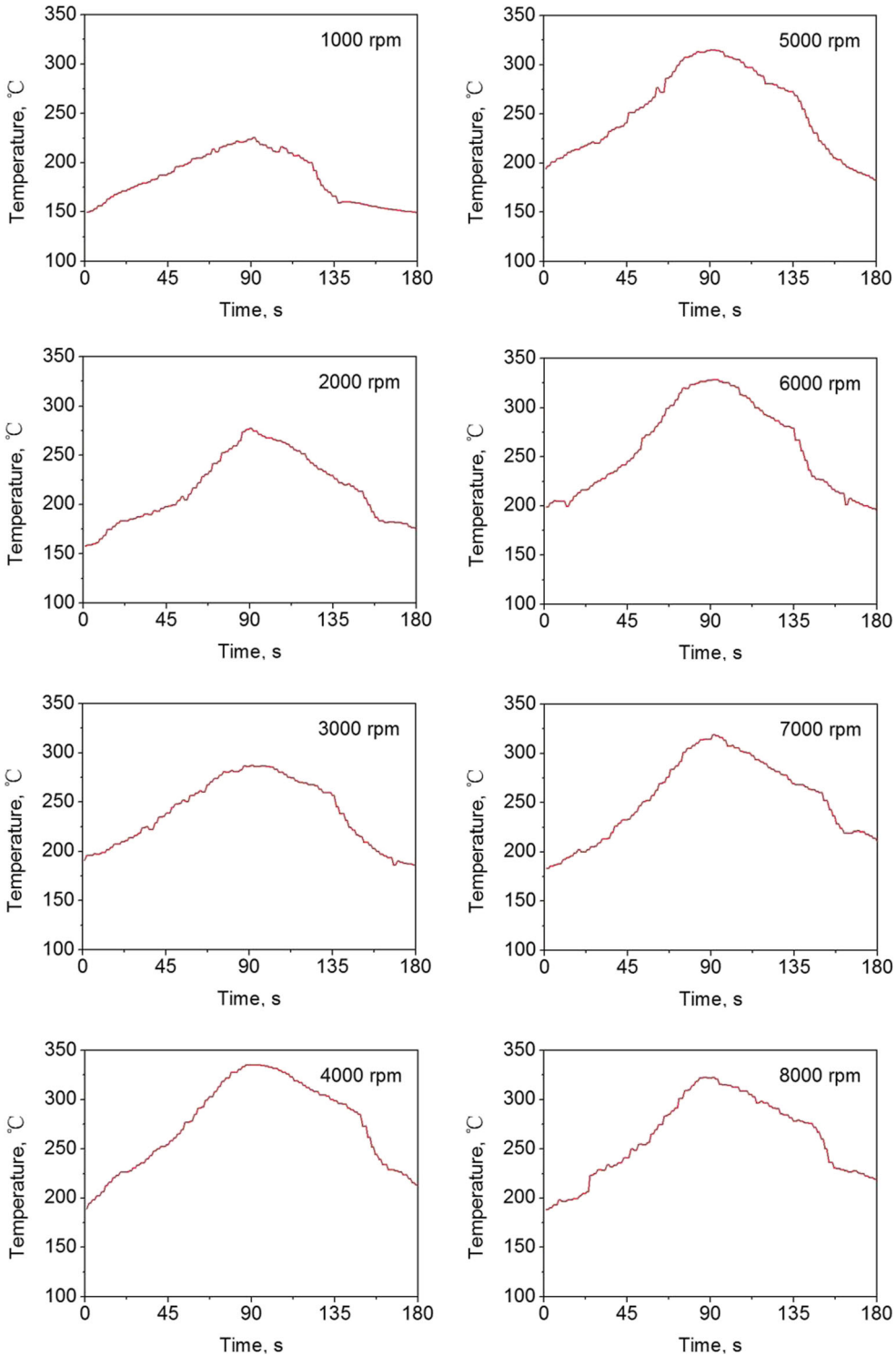

Fig. 7 Welding thermal cycles obtained at different rotation speeds

leading to a total nugget height of about 2.4 mm. In comparison, no secondary material flow takes place below the pin in this study, whereas the large-height nuggets are still produced in HRS-FSW joints. The large nugget height is also a reflection of the strong material flow during HRS-FSW. In C-FSW, the pin length of tool is generally set to be about 0.1–0.3 mm shorter than the plate thickness [13, 14]. Apparently, this is not applicable for the HRS-FSW process. The relationship between nugget height and pin length is very important for the design of HRS-FSW tool and needs further investigation by combining the experiments and numerical modeling.

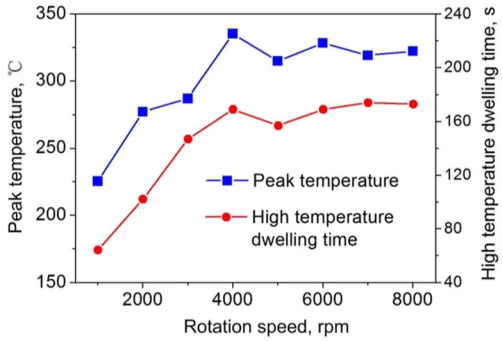

Fig. 8 Peak temperature and high-temperature dwelling time above 200 °C measured at different rotation speeds

3.2 Welding thermal cycles

Figure 7 presents the welding thermal cycles measured at different rotation speeds. For each rotation speed, the measurement location experienced a heating state and then a cooling state as the tool passed, leading to a peak temperature and a high temperature dwelling time in the welding thermal cycle. For aluminum alloys, the dynamically recrystallized grains can grow statically above $0.5T_m$ (T_m being the absolute melting temperature of BM) [15]. Hence, the peak temperature and the high temperature dwelling time above $0.5T_m$ (200 °C) are plotted against rotation speed, as shown in Fig. 8. Since the measurement locations of welding thermal cycles, lying at the workpiece bottom surface beneath tool pin, are relatively far from the tool shoulder, the measured peak temperatures are only between 225 and 335 °C. The peak temperature and high temperature dwelling time both increase progressively from 1000 to 4000 rpm, but they vary slightly above 4000 rpm. This is surprising, given that the heat input would be expected to continue to increase at higher rotation speeds.

In Schmidt et al.'s model [16], the total heat generation from frictional and plastic dissipation during FSW can be synthetically described by the following relationship:

$$q = \omega r \tau(T) \tag{1}$$

where ω is the tool rotation speed, r is the radius, and $\tau(T)$ is the temperature dependent material shear stress.

From this relationship, the effect of rotation speed on welding temperature during HRS-FSW can be easily understood. In the relatively low rotation speed range of 1000–4000 rpm, the rotation speed is the dominant factor that controls the heat generation, and thus, the peak temperature and high-temperature dwelling time are both improved with increasing rotation speed. However, it should be noted that the increase of rotation speed simultaneously lowers the material shear stress due to the strong tool stirring action. As the rotation speed reaches above 4000 rpm, the material shear stress is decreased significantly. The main factor that influences the heat input is then changed from rotation speed to material shear stress, which finally leads to the relatively steady state of temperature evolution with rotation speed.

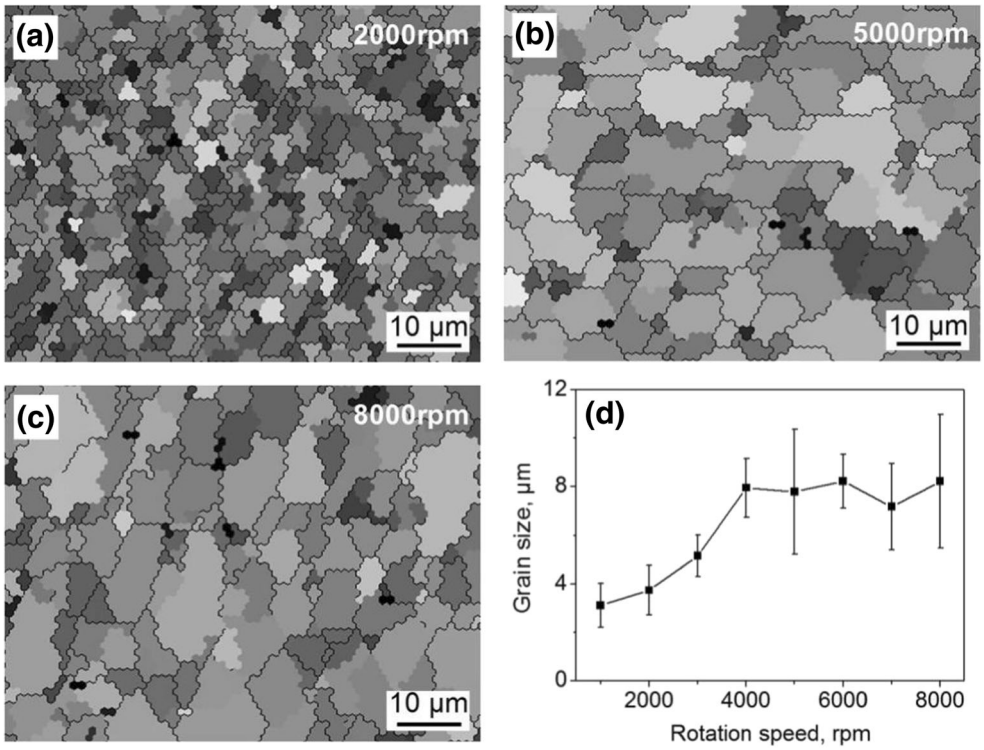

Fig. 9 Grain structures of the nugget zones obtained at different rotation speeds. **a** 2000 rpm. **b** 5000 rpm. **c** 8000 rpm. **d** Evolution of grain size with rotation speed

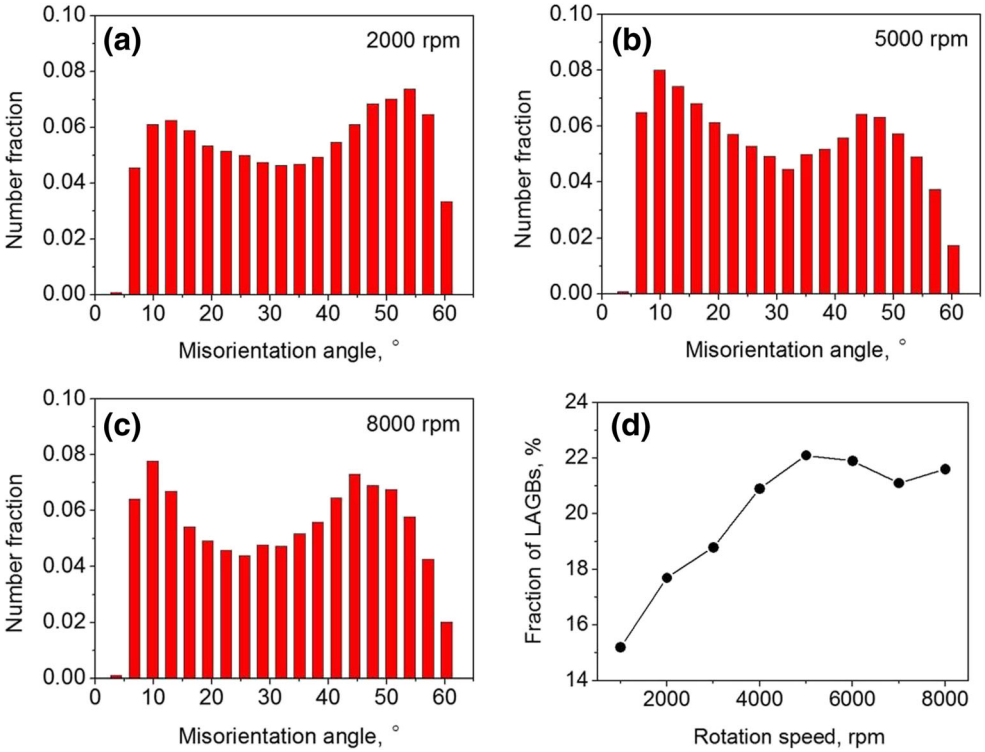

Fig. 10 Misorientation angle distribution of the nugget zones obtained at different rotation speeds. **a** 2000 rpm. **b** 5000 rpm. **c** 8000 rpm. **d** Evolution of misorientation angle distribution with rotation speed

The rotation speed generally dominates the heat generation during C-FSW, and the welding temperature is mostly found to be improved with increasing rotation speed [17–19]. The correlations between process parameters and welding temperatures in HRS-FSW are rarely documented in the published literature. The present study confirms a different rotation speed-welding temperature relationship in HRS-FSW from that in C-FSW. The results indicate that the welding

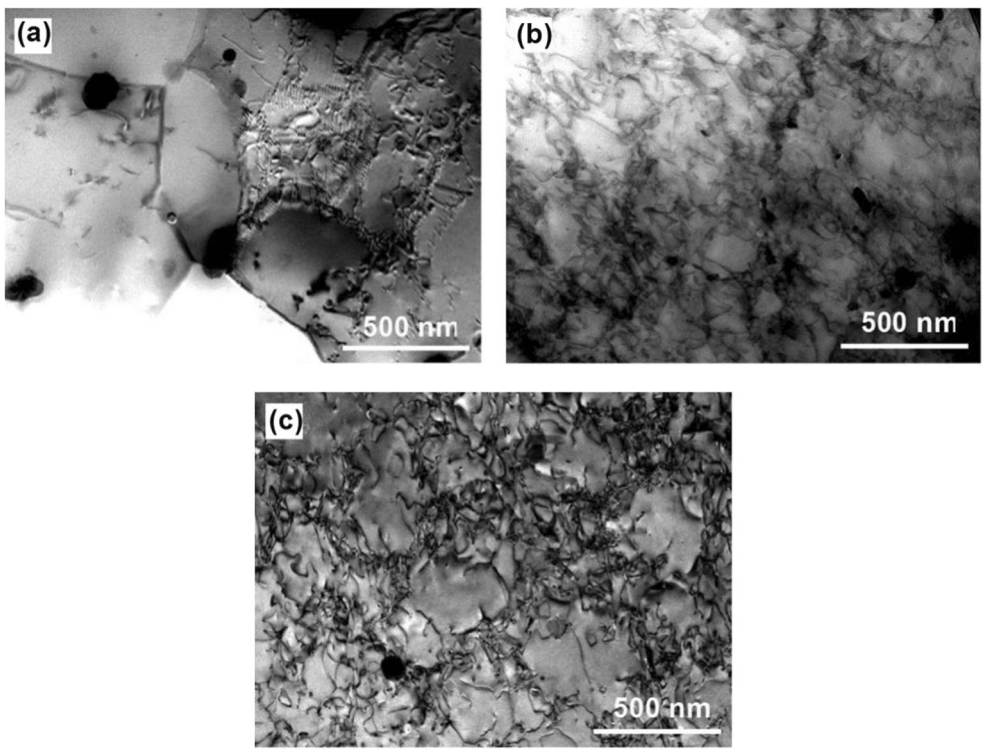

Fig. 11 TEM microstructures of the nugget zones obtained at different rotation speeds. **a** 2000 rpm. **b** 5000 rpm. **c** 8000 rpm

temperature can achieve a steady state during HRS-FSW if the rotation speed is improved to a certain high level, which is intrinsically resulted from the lowering of the material shear stress.

3.3 Microstructure evolutions

The special temperature-rotation speed relationship should have effects on the microstructure evolutions. The grains and substructures of nugget zones are thereby analyzed to clarify the nugget microstructure features. The grains were revealed by electron back-scattered diffraction (EBSD). The EBSD data was collected using a JEOL JSM-7001F scanning electron microscope and processed with TSL OIM Analysis 6 software. In contrast to the BM, the nugget grains present fine equiaxed structures due to dynamically recrystallization (see Fig. 9a–c). The grain size increases evidently from 1000 to 4000 rpm, but after that, it changes slightly with the rotation speed variation (see Fig. 9d).

Figure 10 displays the corresponding misorientation angle distribution of the nugget grains shown in Fig. 9. The misorientation angle was calculated using the EBSD data at two adjacent measurement positions. The low-angle grain boundaries (LAGBs, the grain boundaries with the misorientation ranging from 2° to 15°) reflect the substructures within the nugget grains. All the nuggets contain higher fractions of LAGBs than the BM (see Figs. 10a–c and 1b, indicating that a large amount of substructures have been formed in the nuggets during HRS-FSW. The fraction of LAGBs is progressively improved from 1000 to 4000 rpm, but it is kept at a nearly steady state between 4000 and 8000 rpm (see Fig. 10d).

The transmission electron microscopy (TEM) microstructures of BM and nugget zones were observed by PHILIPS CM12 to further illustrate the substructure features. Compared with BM, the second phase particles are nearly all dissolved into the matrix in the nuggets under the elevated temperature. Furthermore, all the nuggets possess higher dislocation densities than the BM (see Figs. 11 and 1c. This should be attributed to the fact that dislocations are continuously generated by the intense plastic deformation during FSW [20]. Obviously, the dislocation densities at 5000 and 8000 rpm are higher than that at 2000 rpm. The slip and pile-up of the generated dislocations promote the formation of recovered structures, and thus, the weld nuggets show larger fractions of LAGBs at higher rotation speeds.

The nugget microstructures, including the grains and substructures (LAGBs and dislocations), are actually formed under the thermal and stirring effects of the tool during the welding. Thus, the nugget microstructures are synthetically affected by the welding temperature and the stain rate of plastic material. With increasing rotation speed, the evolution trends of grain size and distribution density of substructures both resemble that of welding temperature. This implies that

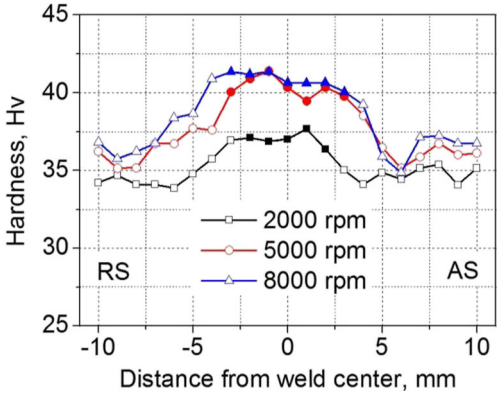

Fig. 12 Hardness profiles produced at different rotation speeds. Note that the data points marked by *solid symbols* are located in the weld nugget zones

the nugget microstructure evolution during HRS-FSW appears to be more sensitive to welding temperature as the rotation speed varies. The welding temperature also commonly acted as a dominant factor that controlled the nugget microstructure evolution in C-FSW [21], the difference is that the grain size and substructure distribution density in nugget zones of C-FSW joints both tended to be consistently improved with increasing rotation speed [22–24].

3.4 Hardness distributions

To correlate the microstructures with the weld properties, hardness measurements on weld cross sections were conducted at different rotation speeds. Some typical examples are given in Fig. 12. Moving inward from BM to weld center, the hardness profiles start to increase as the nugget zones are approached on both sides of the welds. The higher hardness of nuggets relative to BM is typical for the FSW joints of non-heat-treatable aluminum alloys [3], which should be attributed to the work hardening and grain refinement. The data points are identified by solid symbols in Fig. 12 represent the hardness of the nugget zones. For a given rotation speed, the hardness values measured at the nugget zone are averaged to evaluate the nugget properties. The evolution of nugget hardness

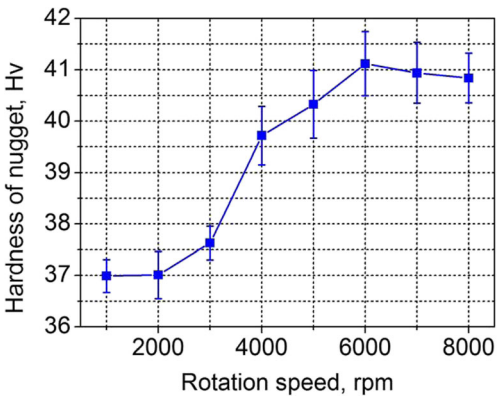

Fig. 13 Evolution of nugget hardness with rotation speed

with rotation speed is plotted in Fig. 13. It is clear that with increasing rotation speed, the nugget hardness exhibits the similar evolution trend with the nugget structure morphology, i.e., first increases from 1000 to 4000 rpm and then shows a slight variation trend from 4000 to 8000 rpm. This means that increasing the rotation speed to a certain level can cause an improvement in nugget properties. In the meanwhile, it also shows that the high-quality HRS-FSW joints can be formed at a larger range of rotation speeds.

The variation characteristic of nugget hardness with rotation speed is essentially related to the microstructure evolution. The nugget microstructures contain grains and substructures. Since the increase of grain size tends to reduce the hardness according to the Hall-Petch relationship, the hardness improvement at higher rotation speeds should be induced by high distribution densities of substructures rather than the coarsened grains. The dislocation-dominant strengthening mechanism for nugget zone was commonly observed in the C-FSW of aluminum alloys [25, 26], and this study demonstrates that it can also be present in the HRS-FSW of aluminum alloys.

Overall, sound HRS-FSW joints are produced in a wide rotation speed range in this paper. The effect of rotation speed on thermal and mechanical behaviors of nugget zone is found to reach a steady state when the rotation speed is improved to a certain high level. Such high-level rotation speeds not only enlarge the nugget size but also can improve the nugget properties through the enhancement of strain hardening. In regard to the non-heat-treatable aluminum alloys, this study also confirms that the HRS-FSW is tolerant of variation in rotation speed for high-quality joints, which provides a fundamental technological understanding for the process control and application.

4 Conclusions

Based on the present investigation, the conclusions of significance are drawn as follows:

(1) The nugget width varies slightly from 1000 to 4000 rpm, but it largely increases by about 4.5 mm when the rotation speed is increased to the range of 5000–8000 rpm. Compared with C-FSW, the nugget heights of HRS-FSW joints are remarkably larger than pin length. The differences between the nugget heights and pin length reach about 1.5 mm.

(2) The welding temperature is gradually improved from 1000 to 4000 rpm. Nevertheless, with further increasing rotation speed, the material shear stress would decrease to a low level and become the main factor that governs the heat generation, leading to a relatively steady state of welding thermal cycles.

(3) Under the high rotation speed condition, the nugget microstructure evolution with rotation speed is found to be sensitive to the welding temperature. With increasing rotation speed, the evolution trends of grain size and distribution density of substructures resemble that of welding temperature.

(4) Increase of rotation speed to a certain level benefits the strength improvement of the nugget zone. By increasing the rotation speed above 4000 rpm, the nugget hardness is evidently improved due to the enhancement of strain hardening at higher rotation speeds.

Acknowledgements The authors are grateful to be supported by National Natural Science Foundation of China (Grant No. 51505471) and Innovation Fund from Youth Innovation Promotion Association, Chinese Academy of Sciences (Grant No. 2015162).

References

1. Nandan R, Debroy T, Bhadeshia HKDH (2008) Recent advances in friction-stir welding—process, weldment structure and properties. Prog Mater Sci 53:980–1023
2. Silva ACF, Braga DFO, Figueiredo MAV d, Moreira PMGP (2015) Ultimate tensile strength optimization of different FSW aluminium alloy joints. Int J Adv Manuf Technol 79:805–814
3. Cam G, Mistikoglu S (2014) Recent developments in friction stir welding of Al-alloys. J Mater Eng Perform 23:1936–1953
4. Azimzadegan T, Serajzadeh S (2010) An investigation into microstructures and mechanical properties of AA7075-T6 during friction stir welding at relatively high rotational speeds. J Mater Eng Perform 19:1256–1263
5. Cook GE, Crawford R, Clark DE, Strauss AM (2004) Robotic friction stir welding. Ind Robot 31:55–63
6. Ding J, Carter R, Lawless K, Nunes A, Russell C, Suits M, Schneider J (2006) Friction stir welding flies high at NASA. Weld J 85:54–59
7. Banwasi N (2005) Mechanical testing and evaluation of high-speed and low-speed friction stir welds. Dissertation, Wichita State University
8. Widener CA, Talia JE, Tweedy BM, Burford DA (2006) High-rotational speed friction stir welding with a fixed shoulder. 6th International Symposium on Friction Stir Welding, Session 8B, Nr Montréal, Canada
9. Nicholas T (2009) Advances in high rotational speed-friction stir welding for NAVAL applications. Dissertation, Wichita State University
10. Crawford R, Bloodworth T, Cook GE, Strauss AM (2006) High speed friction stir welding process modeling. 6th International Symposium on Friction Stir Welding, Session 12A, Nr Montréal, Canada
11. Doude H, Schneider J, Patton B, Stafford S, Waters T, Varner C (2015) Optimizing weld quality of a friction stir welded aluminum alloy. J Mater Process Technol 222:188–196
12. Buchibabu V, Reddy GM, Kulkarni D, De A (2016) Friction stir welding of a thick Al-Zn-Mg aluminum alloy. J Mater Eng Perform 25:1163–1171
13. Dubourg L, Dacheux P (2006) Design and properties of FSW tools: a literature review. 6th International Symposium on Friction Stir Welding, Session 1, Nr Montrral, Canada

14. Zhang YN, Cao X, Larose S, Wanjara P (2012) Review of tools for friction stir welding and processing. Can Metall Q 51:250–261
15. Sato YS, Sugiura Y, Kokawa H (2003) Hardness distribution and microstructure in friction stir weld of aluminum alloy 5052. 4th International Symposium on Friction Stir Welding, Poster presentation, Utah, USA
16. Schmidt HB, Hattel JH (2008) A thermal-pseudo-mechanical model for the heat generation in friction stir welding. 7th International Symposium on Friction Stir Welding, Session 2B, Awaji Island, Japan
17. Hao HL, Ni DR, Huang H, Wang D, Xiao BL, Nie ZR, Ma ZY (2013) Effect of welding parameters on microstructure and mechanical properties of friction stir welded Al-Mg-Er alloy. Mater Sci Eng A 559:889–896
18. He J, Ling ZM, Li HM (2016) Effect of tool rotational speed on residual stress, microstructure, and tensile properties of friction stir welded 6061-T6 aluminum alloy thick plate. Int J Adv Manuf Technol 84:1953–1961
19. Jamshidi AH, Serajzadeh S, Kokabi AH (2012) Experimental and theoretical evaluations of thermal histories and residual stresses in dissimilar friction stir welding of AA5086-AA6061. Int J Adv Manuf Technol 61:149–160
20. Su JQ, Nelson TW, Mishra R, Mahoney M (2003) Microstructural investigation of friction stir welded 7050-T651 aluminum. Acta Mater 51:713–729
21. Jamshidi AH, Serajzadeh S, Kokabi AH (2011) Theoretical and experimental investigation into friction stir welding of AA 5086. Int J Adv Manuf Technol 52:531–544
22. Zhang HJ, Liu HJ, Yu L (2011) Microstructure and mechanical properties as a function of rotation speed in underwater friction stir welded aluminum alloy joints. Mater Des 32:4402–4407
23. Wang T, Zou Y, Matsuda K (2016) Micro-structure and micro-textural studies of friction stir welded AA6061-T6 subjected to different rotation speeds. Mater Des 90:13–21
24. Hou JC, Liu HJ, Zhao YQ (2014) Influences of rotation speed on microstructures and mechanical properties of 6061-T6 aluminum alloy joints fabricated by self-reacting friction stir welding tool. Int J Adv Manuf Technol 73:1073–1079
25. Svensson LE, Karlsson L, Larsson H, Karlsson B, Fazzini M, Karlsson J (2000) Microstructure and mechanical properties of friction stir welded aluminium alloys with special reference to AA 5083 and AA 6082. Sci Technol Weld Join 5:285–296
26. Amini S, Amiri MR, Barani A (2015) Investigation of the effect of tool geometry on friction stir welding of 5083-O aluminum alloy. Int J Adv Manuf Technol 76:255–261